

Strong plasmon absorption in InN thin films

A. Dixit, C. Sudakar, J. S. Thakur, K. Padmanabhan, Sanjiv Kumar, R. Naik, V. M. Naik, and G. Lawes

Citation: *Journal of Applied Physics* **105**, 053104 (2009); doi: 10.1063/1.3088879

View online: <http://dx.doi.org/10.1063/1.3088879>

View Table of Contents: <http://scitation.aip.org/content/aip/journal/jap/105/5?ver=pdfcov>

Published by the [AIP Publishing](#)

Articles you may be interested in

[High-precision determination of lattice constants and structural characterization of InN thin films](#)

J. Vac. Sci. Technol. A **24**, 275 (2006); 10.1116/1.2167970

[Publisher's Note: "Single-crystalline InN films with an absorption edge between 0.7 and 2 eV grown using different techniques and evidence of the actual band gap energy" \[Appl. Phys. Lett. 83, 4788 \(2003\)\]](#)

Appl. Phys. Lett. **84**, 452 (2004); 10.1063/1.1644578

[Infrared reflection characteristics in InN thin films grown by magnetron sputtering for the application of plasma filters](#)

J. Appl. Phys. **92**, 3683 (2002); 10.1063/1.1506199

[Optical constants of InN thin films on \(111\) GaAs grown by reactive magnetron sputtering](#)

J. Appl. Phys. **91**, 9803 (2002); 10.1063/1.1481189

[Bandtail characteristics in InN thin films](#)

Appl. Phys. Lett. **80**, 2063 (2002); 10.1063/1.1464219

The advertisement features a dark blue background with a glowing blue light effect. On the left, there is a stylized image of a film strip with a purple and yellow textured surface. The text is centered and reads: "Not all AFMs are created equal" in orange, "Asylum Research Cypher™ AFMs" in white, and "There's no other AFM like Cypher" in orange. At the bottom left, the website "www.AsylumResearch.com/NoOtherAFMLikeIt" is written in white. At the bottom right, the Oxford Instruments logo is shown, consisting of the word "OXFORD" in a large font above "INSTRUMENTS" in a smaller font, with the tagline "The Business of Science®" below it.

Strong plasmon absorption in InN thin films

A. Dixit,¹ C. Sudakar,¹ J. S. Thakur,¹ K. Padmanabhan,¹ Sanjiv Kumar,³ R. Naik,¹ V. M. Naik,² and G. Lawes^{1,a)}

¹Department of Physics and Astronomy, Wayne State University, Detroit, Michigan 48201, USA

²Department of Natural Sciences, University of Michigan-Dearborn, Dearborn, Michigan 48128, USA

³NCCCM, Bhabha Atomic Research Centre, ECIL Post, Hyderabad 500062, India

(Received 20 October 2008; accepted 23 January 2009; published online 9 March 2009)

We have fabricated InN thin films using rf magnetron sputtering from an indium (In) metal target. Optical and electrical measurements show that these as-grown films are *n*-type with carrier concentrations ranging from 10^{20} to 10^{21} cm⁻³. This variation in carrier density is produced by controlling the conditions during the deposition. We used Rutherford backscattering spectrometry to identify possible sources for *n*-type carriers. We found that in addition to strong direct bandgap optical absorption ranging from 1.4 to 2.0 eV, a large plasmon absorption peak in the infrared region (0.45–0.8 eV) is also observed. This tunable IR absorption suggests that these highly degenerate InN films could be used for a number of applications, including optical filters and infrared devices.

© 2009 American Institute of Physics. [DOI: 10.1063/1.3088879]

I. INTRODUCTION

Group III-nitrides are normally wide band gap semiconducting materials, suitable for applications in ultraviolet and visible spectrum optical devices and high power electronics. Among these nitrides, only InN is known to have a small intrinsic band gap (0.7 eV) and is considered to be a promising material for optoelectronics and other devices.^{1,2} Due to a smaller electron effective mass than the other III-nitrides, InN exhibits a higher mobility and higher saturation velocity, making it attractive for a number of electronic applications. Theoretically estimated maximum values of mobility for InN and GaN at 300 K are approximately 4400 and 1000 cm²/V s respectively, while the values at 77 K exceed 30 000 and 6000 cm²/V s.¹ InN also exhibits a very high peak velocity 4.2×10^7 cm/s, at room temperature.¹ Taken in aggregate, these values suggest that the transport characteristics of InN may be superior to those of GaN and GaAs over a wide range of temperatures.¹

Although the theoretically predicted parameters for InN are extremely promising for applications, InN films fabricated by many methods are often of poor quality, leading to degradation of properties. The fabrication of high quality crystalline InN films is challenging because of the large lattice mismatch with many commonly used substrates, the low dissociation temperature, and stoichiometric instability promoting the inclusion of oxygen impurities. During synthesis, this leads to the introduction of variety of defects during synthesis, including randomly distributed charged impurities, charge dislocation lines, grain boundaries, surface charge defects, vacancies, and oxygen impurities. The nature of the defects introduced in the samples depends strongly on the fabrication technique. Molecular beam epitaxy (MBE) generally produces very high quality samples with a low carrier density,^{3,4} while other techniques, including plasma source

MBE, metal organic chemical vapor deposition, and sputtering, normally produce lower quality samples having higher carrier densities.⁵⁻⁷

The high carrier densities, up to $N_e \sim 10^{21}$ cm⁻³, in these lower quality films suggest that there is a much higher concentration of donor defects compared to other III-nitride films. The origin of these donor defects is unclear and is attributed to oxygen incorporation or nitrogen native defects, among other possibilities.¹ While this high carrier concentration is contraindicated for many applications, these samples can exhibit intense plasmon excitations similar to those found in metals.⁸ These InN films can therefore act as strong tunable absorbers of optical/infrared signals when the signal frequency matches the plasmon frequency of the sample. For small carrier densities, the absorption cross section for plasmon excitations is very small. However, if the absorption coefficient for the plasmon excitation becomes comparable to that of direct bandgap excitations, then these plasmon excitations could potentially be used for a number of applications that currently rely on direct bandgap absorption. Plasmon absorption offers a distinct advantage over direct bandgap absorption because the frequency response can be tuned continuously by varying the carrier density.

In the following, we present experimental evidence suggesting that highly degenerate InN films could potentially be used as a plasma filter material in thermophotovoltaic systems^{9,10} or in other optical applications. We illustrate this effect by presenting reflectance and absorption spectra of various degenerate InN films fabricated using RF magnetron sputtering.

II. EXPERIMENTAL DETAILS

InN thin films with different carrier concentrations were grown using reactive rf (13.56 MHz) magnetron sputtering system with a high purity (5N) indium metal target onto *c*-sapphire substrates. The growth temperature of these films was kept at $\sim 470 \pm 5$ °C using deposition parameters that

^{a)}Electronic mail: glawes@wayne.edu.

TABLE I. Growth parameters and physical properties of the films.

Sample No.	Growth parameters			Optical band edge	Thickness	Carrier density	Electron mobility	Plasmon frequency	Plasmon damping
	Partial pressure (Torr)	Power (W)	Time (min)	E_g (eV)	t (nm)	N (cm ⁻³)	μ (cm ² /V s)	ω_p (eV)	γ (eV)
1	0	1.5×10^{-2}	100	30	194	3.84×10^{20}	21.5	0.459	0.155
2	0	3.0×10^{-2}	100	30	200	5.44×10^{20}	20.7	0.545	0.161
3	5×10^{-3}	1.0×10^{-2}	100	30	790	9.78×10^{20}	26.8	0.731	0.124
4	1×10^{-2}	5.0×10^{-3}	40	30	840	1.11×10^{21}	24.5	0.781	0.136
5	1×10^{-2}	5.0×10^{-3}	40	04	71	1.26×10^{21}	9.6	0.831	0.347

were optimized for preparing InN thin films. These films were fabricated using N₂ as the reactive gas and Ar as sputtering gas at a working pressure of 1.5×10^{-2} torr. The growth parameters, including sputtering time and partial pressure of reactive and sputtering gases, were adjusted to control the carrier concentration of InN thin films. The growth parameters and corresponding properties of these films are summarized in Table I.

The crystalline quality of these InN/Sap films was investigated using x-ray diffraction (XRD) and cross-sectional scanning electron microscopy (SEM) analysis. The XRD patterns for these InN films are shown in Figs. 1(a) and 1(b). The XRD pattern consists of intense peaks at $2\theta=31.43^\circ$ and 65.4° corresponding to the (002) and (004) reflections for hexagonal wurtzite InN thin films, indicating that films are highly textured and *c*-axis oriented. The *c*-axis lattice parameter of these InN films, obtained from the XRD patterns is ~ 5.69 Å, which is in good agreement with the reported literature values.^{11,12} A representative cross-sectional SEM image of the InN/Sap film with the highest carrier concentration is shown in Fig. 1(c). The cross-sectional analysis of these

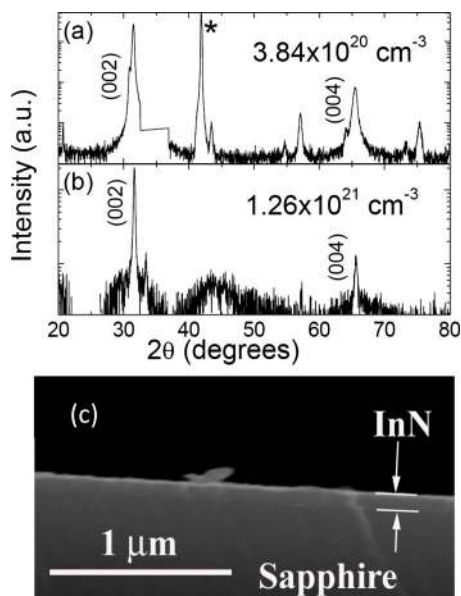


FIG. 1. (Color online) XRD spectra of InN thin films having (a) lowest carrier concentration and (b) highest carrier concentration. The * indicates the substrate peak due to the Al₂O₃ (0006) reflection. The small anomaly near 35° in panel (a) represents an instrumental error. (c) Cross-sectional SEM image of the InN/sapphire thin film with $n=1.26 \times 10^{21}$ cm⁻³.

films indicates a sharp interface between the film and substrate with well oriented columnar growth along the *c*-axis. We also carried out high resolution transmission electron microscopy (HRTEM) of these films. Both InN thin films with high and low carrier concentrations show highly oriented columnar grains of the InN. These columnar structures are ~ 50 nm wide and are oriented along the *c*-axis of the wurtzite structure perpendicular to the substrate plane. Secondary inclusions such as In (Ref. 13) and In₂O₃ (Ref. 7) have been reported to form within the InN lattice. However, for our samples we observe highly crystalline columnar grains using HRTEM with no discernible defects or secondary inclusions, as shown in Fig. 2.

We investigated the source of the *n*-type carriers in these highly degenerate films by determining their composition using Rutherford backscattering spectrometry (RBS). We focused on the highest carrier concentration film, since this would be expected to show the largest deviation from stoichiometry. The RBS data acquired using a standard detector (angle of 140°), a 180° annular detector and a 40° annular detector using a ⁴He⁺, 2 MeV beam from a Van de Graaff accelerator are shown in Fig. 3. A nuclear data function (NDF) simulation package was used to simulate the experimental results and to estimate the In to N ratio. This estimate yields the result that the In:N ratio is 47:53. This excess nitrogen in this film suggests that other compensating defects could also be responsible for the excess charge carriers.¹ Preliminary data on samples prepared under nitrogen rich deposition conditions, which have low carrier concentrations, show that the In:N ratio diverges even more from stoichiometry, suggesting that acceptor-type defects such as In vacancies (V_{In}^{3-}) becoming more favorable or presence of oxygen may be influencing the carrier density. We therefore believe that excess nitrogen plays at most a minimal role in modify-

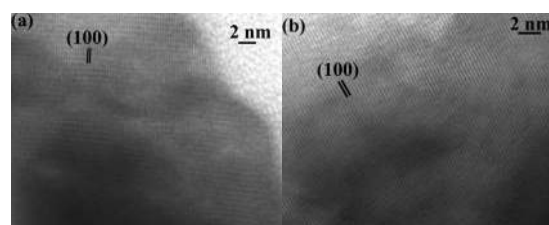


FIG. 2. HRTEM images of (a) the lowest carrier concentration film and (b) the highest carrier concentration film.

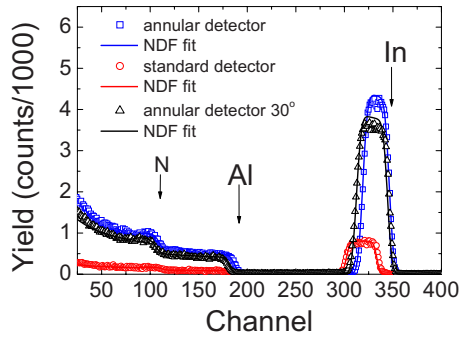


FIG. 3. (Color online) RBS spectra highest carrier concentration thin film with a standard detector of 140° angle (red circle), 180° annular detector (blue square), and 30° annular detector (black triangle). Symbols are experimental spectra. The fit using the NDF simulation is shown as a line.

ing the carrier concentration, which is rather determined mainly by the presence of oxygen in the samples.

Raman spectroscopy measurements were carried out at room temperature using a 514.5 nm excitation wavelength to study the lattice modes of these samples. These spectra are shown in Figs. 4(a) and 4(b) for the films having lowest and highest carrier densities, respectively. Factor group analysis at the Γ point in hexagonal InN predicts a total of six allowed Raman active modes,¹³ of which three are typically observed for c -axis oriented InN films, namely, the E_2 (low), E_2 (high), and A_1 (LO) which occur near 90, 490, and 580 cm^{-1} , respectively.^{14–16} The Raman spectra of these films contain additional peaks close to 128, 305, and 370 cm^{-1} which are characteristics of bcc In_2O_3 ,^{7,17–19} the presence of In_2O_3 secondary phases is consistent with observations of a finite oxygen concentration in these samples. Oxygen impurities have been proposed as a mechanism for producing the high carrier concentration in InN,¹ so the excess oxygen in these samples could be responsible for the degenerate nature of these films.⁷

In an ideal InN lattice, the B_1 Raman mode is silent in Raman. However, this mode can be observed in defective InN samples.²⁰ The excess oxygen in these sputtered films may be sufficient to distort the InN lattice and break the local crystal symmetry. This can allow the excitation of the B_1 (low) and B_1 (high) modes at ~ 200 and 565 cm^{-1} , respectively. We note that some of the Raman active modes are

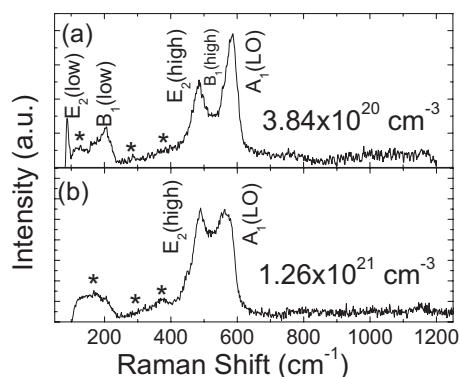


FIG. 4. Raman spectra of InN thin films with (a) lowest carrier concentration and (b) highest carrier concentration. The * corresponds to the peaks from In_2O_3 at 129, 303, and 375 cm^{-1} .

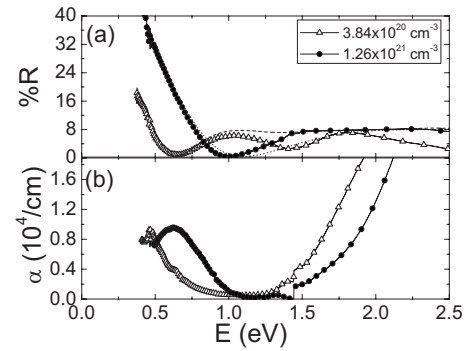


FIG. 5. Optical spectra of InN/Sap thin films (a) reflectance and (b) absorption spectra. Closed (open) symbols and dotted (dashed) lines show the experimental data and simulated spectrum for the films having a carrier concentration of $1.26 \times 10^{21}\text{ cm}^{-3}$ ($3.84 \times 10^{20}\text{ cm}^{-3}$). In Fig. 4(b) the jumps are due to grating changes at these wavelengths.

absent in these highly disordered films, as shown in Fig. 4(b). This strong disorder has two main effects on the properties of the films: the disorder broadens the Raman modes due to lattice distortions and the disorder is also a source of additional charge carriers. These carriers can strongly interact with certain optical modes and influence their spectral characteristics. Figure 4(b) shows a possible evidence for this coupling through the suppression of the E_2 (low) mode and broadening of the B_1 (low), E_2 (high), and A_1 (LO) modes.

We have also investigated various optical properties of these InN films using UV-vis-NIR spectroscopy. Optical transmittance and reflectance [Fig. 5(a)] spectra were measured from 175 to 3300 nm for all samples to determine the absorbance and extract the absorption coefficient, α . Figure 5(b) shows the absorption coefficient for the lowest and highest carrier density films. Typically the optical response in InN consists of only direct bandgap absorption located at an energy corresponding to the bandgap energy plus the Moss–Burstein shift.^{11,21} It is interesting to note that in addition to the direct bandgap absorption there is an additional absorption at lower energies. This absorption, which is attributed to plasmon excitations, is found to be as strong as the direct bandgap absorption. In these samples the lower energy absorption peak varies from 0.45 to 0.8 eV, which lies in the infrared region of the electromagnetic spectrum. We are able to tune the carrier density, which, in turn, determines the plasmon energy, by controlling the partial pressures of N_2 and Ar during deposition.

III. RESULTS AND DISCUSSION

Both reflectance curves in Fig. 5(a) exhibit a large reflection edge due to the plasmon excitation in the lower energy portion of the spectrum. At higher energies, we observe well defined oscillations due to optical interference between the waves reflected from the substrate interface and the surface. The period of these oscillations is related to the film thickness; we used this interference to determine the sample thickness using the known dielectric constant. We analyzed the reflectance spectra using the Drude model for the dielectric function^{22,23} where contributions from the LO phonons and plasmon excitation are taken into account according to

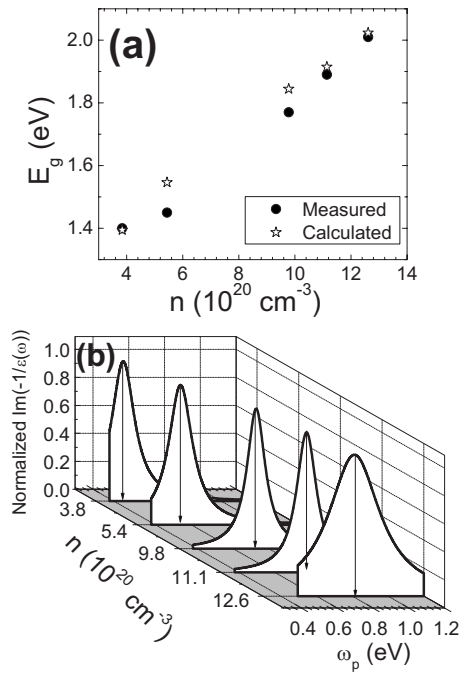


FIG. 6. (a) Measured and computed values for the optical absorption edge vs carrier concentration extracted from the plasmon resonance peak. (b) Normalized plot of $\text{Im}(-1/\epsilon(\omega))$ vs ω_p (eV) plot for different InN/Sap thin films (arrows guiding corresponding ω_p values).

$$\epsilon(\omega) = \epsilon_\infty \left[1 + \frac{\omega_{\text{LO}}^2 - \omega_{\text{TO}}^2}{\omega_{\text{TO}}^2 - \omega^2 - i\omega\gamma} - \frac{\omega_p^2}{\omega^2 + i\omega\Gamma} \right]. \quad (1)$$

Here $\omega_{\text{TO}}/\gamma$ and $\omega_{\text{LO}}/\Gamma$ are the TO and LO frequency/damping, respectively. $\omega_p = (4\pi N_e e^2 / m^* \epsilon_o)^{1/2}$ is the plasmon frequency, N_e is the electron density, m^* is the electron effective mass, and ϵ_o is the static dielectric constant. The phonon frequencies are determined using our Raman data, while the damping factors are considered as adjustable parameters to fit the reflectance spectra. In these films the plasmon energies are much larger than the LO-phonon energy so the coupling between the fundamental modes of plasmon and LO phonons is negligible.

We estimated the carrier concentration of the films using the measured plasmon frequency. These values agree well with those determined from Hall electrical measurements, although in the following we analyze our results using the plasmon frequency values for carrier concentration. The absorption coefficients plotted in Fig. 5(b), show two separate absorption processes in these films, namely, plasmon due to excitations and excitation across the bandgap. Between the plasmon and bandgap excitation regions there is an ~ 1 eV wide transparent portion of the spectrum having very small absorption. Changing the carrier concentration by modifying the deposition conditions leads to a change in the plasmon frequency, and also to a change in the optical absorption edge. In Fig. 6(a) we plot the measured value of the optical absorption edge together with the calculated value based on the plasmon values of the carrier concentration in the framework described below. The good agreement between these measured and calculated values demonstrates that the optical absorption edge and plasmon frequency are both connected to the carrier density. These experiments suggest that the

transparent region in these highly degenerate InN films can be tuned by varying the carrier concentration. This could allow these materials to be used as optical filters or in other optoelectronic applications.

The plasmon excitations in these samples can be understood from the dielectric response function $\epsilon(\omega)$ using $\text{Im}[-1/\epsilon(\omega)]$.²⁴ In Fig. 6(b) we plot the calculated resonances due to plasmon absorption resonances, $\text{Im}[-1/\epsilon(\omega)]$, which lie in the infrared region (0.45–0.8 eV) of the electromagnetic spectrum for these degenerate samples. The half width of the Lorentzian line shape of the absorption peak provides a measure of the plasmon damping due to electron scattering from the defects and lattice phonons. The variations in the widths of these peaks are consistent with the variation in the sample disorder seen in the Raman spectra. We note that the plasmon in the film with the highest carrier concentration is the most strongly damped.

We investigated theoretically the shift in the optical absorption edge beyond the true bandgap value E_g for samples having different electron density using Kane's two-band $\mathbf{k}\cdot\mathbf{p}$ model.²⁵ This model takes into account the electron density dependent shift and the nonparabolic conduction band dispersion due to the small bandgap value for the absorption edge. The variation in the optical absorption edge can be written²⁵ as

$$\begin{aligned} \bar{E}_g = E_g + \frac{\hbar^2 k_F^2}{2m_o} + \frac{1}{2} \left(\left[E_g^2 + 4E_p \frac{\hbar^2 k_F^2}{2m_o} \right]^{1/2} - E_g \right) - \frac{2e^2 k_F}{\pi \epsilon_o} \\ - \frac{e^2 k_{TF}}{2\epsilon_o} \left[1 - \frac{4}{\pi} \tan^{-1} \left(\frac{k_F}{k_{TF}} \right) \right]. \end{aligned} \quad (2)$$

The last two terms take into account the renormalization of the bandgap energy due to electron-electron interaction effects. $k_F = (3\pi^2 N_e)^{1/3}$ and $k_{TF} = 2\sqrt{\pi}(k_F m_e^* / 0.53\epsilon_o)$ are the Fermi and Thomas-Fermi wavevectors, respectively. Here, the electron density N_e is estimated from the plasmon resonance. E_p is an energy parameter of the Kane's two-band $\mathbf{k}\cdot\mathbf{p}$ model. In order to evaluate this expression, we have taken $E_g = 0.7$ eV and $E_p = 6.0$ eV. The estimated and experimentally determined values of E_g for samples having different carrier concentrations are in good agreement, as shown in Fig. 6(a).

Optical devices based on absorption generally rely on direct bandgap excitations,^{1,2} having absorption coefficients values on the order of $10^4/\text{cm}$.²⁶ The plasmon absorption coefficient in semiconductors is generally rather small, making this process unsuitable for optical devices. However, we have shown that the absorption coefficient at the plasmon resonance in these degenerate InN films approaches values typical of interband transitions. A relatively narrow plasmon absorption width confirms that these excitations are well defined and allows the optical absorption to be tuned to a narrow energy range. This well defined strong plasmon absorption may be utilized for IR and optical devices replacing the low band gap semiconductors normally used for these applications. These highly degenerate InN films could be incorporated into thermophotovoltaic systems as a plasmon filter. Thermophotovoltaic (TPV) devices consist of two main components: the filtering layer and the absorption layer. The

filtering layer reflects the spectral components having energies less than the bandgap energy of the absorption layer. The bandgap values of TPV systems range from $0.5 \leq E_g \leq 1.1$ eV,²⁷ so to optimize the photovoltaic efficiency, the reflectance edge of the filter should match with the absorption edge of the absorption layer. Taking these factors into consideration, the carrier concentrations and optical mobilities of the optical filter material should be $10^{20} \leq N \leq 10^{21}$ cm⁻³ and $10 \leq \mu \leq 1000$ cm²/V s, respectively.²⁷ These ranges match very well with the carrier density and mobility ranges of the InN samples. By using InN films for these devices, both the reflection and plasmon absorption phenomena can be used to filter out undesired frequency components of the incident signal. Exploiting both the reflection and strong plasmon absorption of degenerate InN films may allow filtering of most of the spurious spectral components, increasing the efficiency of the TPV device.

The optical response of this plasmon excitation is affected by the material properties of the samples. A number of damping mechanisms can broaden the plasmon line shape and limit the sharp absorption at the plasmon resonance. However, most of these damping mechanisms involve plasmon excitations at some finite wave vectors. For example, Landau damping,²⁴ which involves the plasmon merging into the electron-hole pair spectrum, requires plasmon propagation at some critical wave vector. For small but finite wavevectors, plasmons can also decay by exciting two or more electrons, however, contributions to the damping from this process are found to be small.²⁸ Another possible plasmon decay mechanism involves electronic excitations across the bandgap, but this decay path is not feasible in these samples since the plasmon energy falls well below the absorption edge. Because only a small wavevector momentum is transferred to the electrons in these transmission experiments, plasmon damping occurs mainly through scattering with defects. For a given film the type of defects and its concentration are fixed thus pinning the value of damping constant. However, the concentration of defects in each film is different thus producing different plasmon widths. Ideally one would like to have minimum defect concentration, but we believe that these defects are also responsible for producing the high concentration of electrons required for such strong plasmon absorption. Optimizing the properties of these films for efficient absorption will require balancing the requirement for strong plasmon absorption while minimizing defect-driven plasmon damping.

IV. CONCLUSIONS

We have fabricated a number of degenerate InN thin films using reactive rf magnetron sputtering using a high purity indium metal target on *c*-sapphire substrates. Optical and electrical measurements show a wide variation in their carrier concentration values. These films show very strong optical absorption due to degenerate electron gas plasmon, which exhibits absorption coefficients, comparable to those

of the direct bandgap absorption. The plasmon absorption in these films falls in the infrared region (0.45–0.8 eV) of the electromagnetic spectrum. Due to the large and tunable absorption at the plasmon frequencies, these degenerate InN films should be considered as potential materials for infrared devices and optical filters.

ACKNOWLEDGMENTS

This research has been supported by the Institute for Manufacturing Research at Wayne State University and the National Science Foundation through Grant No. DMR-0644823.

- ¹A. G. Bhuiyan, A. Hashimoto, and A. Yamamoto, *J. Appl. Phys.* **94**, 2779 (2003).
- ²S. C. Jain, M. Willander, J. Narayan, and R. V. Overstraeten, *J. Appl. Phys.* **87**, 965 (2000).
- ³V. Y. Davydov, A. A. Klochikhin, R. P. Seisyan, V. V. Emptsev, S. V. Ivanov, F. Bechstedt, J. Furthmuller, H. Harima, A. V. Mudryi, J. Aderhold, O. Semchinova, and J. Garul, *Phys. Status Solidi B* **229**, R1 (2002).
- ⁴J. Wu, W. Walukiewicz, K. M. Yu, J. W. Ager III, E. E. Haller, H. Lu, W. J. Schaff, Y. Saito, and Y. Nanishi, *Appl. Phys. Lett.* **80**, 3967 (2002).
- ⁵D. B. Haddad, J. S. Thakur, V. M. Naik, G. W. Auner, R. Naik, and L. E. Wenger, *Mater. Res. Soc. Symp. Proc.* **743**, L11.22 (2003).
- ⁶T. L. Tansley and C. P. Foley, *J. Appl. Phys.* **59**, 3241 (1986).
- ⁷A. Dixit, C. Sudakar, R. Naik, G. Lawes, and J. S. Thakur, E. F. MaCullen, G. W. Auner, and V. M. Naik, *Appl. Phys. Lett.* **93**, 142103 (2008).
- ⁸S. A. Maier, *Plasmonics: Fundamentals and Applications* (Springer, New York, 2007).
- ⁹T. J. Coutts, *Renewable Sustainable Energy Rev.* **3**, 77 (1999).
- ¹⁰T. J. Coutts, *Sol. Energy Mater. Sol. Cells* **66**, 443 (2001).
- ¹¹K. S. A. Butcher and T. L. Tansley, *Superlattices Microstruct.* **38**, 1 (2005).
- ¹²M. Alevli, R. Atalay, G. Durkaya, A. Weesekara, A. G. U. Perera, N. Dietz, R. Kirste, and A. Hoffmann, *J. Vac. Sci. Technol. A* **26**, 1023 (2008).
- ¹³T. P. Bartel, C. Kisielowski, P. Specht, T. V. Shubina, V. N. Jmerik, and S. V. Ivanov, *Appl. Phys. Lett.* **91**, 101908 (2007).
- ¹⁴V. M. Naik, H. Dai, R. Naik, D. B. Haddad, J. S. Thakur, G. W. Auner, H. Lu, and W. J. Schaff, *Mater. Res. Soc. Symp. Proc.* **831**, E3.16 (2005).
- ¹⁵J. S. Thakur, D. Haddad, V. M. Naik, R. Naik, G. W. Auner, H. Lu, and W. J. Schaff, *Phys. Rev. B* **71**, 115203 (2005).
- ¹⁶T. Inushima, T. Shiraishi, and V. Yu. Davydov, *Solid State Commun.* **110**, 491 (1999).
- ¹⁷E. Kurimoto, M. Hangyo, H. Harima, M. Yoshimoto, T. Yamaguchi, T. Araki, and Y. Nannishi, *Appl. Phys. Lett.* **84**, 212 (2004).
- ¹⁸M. Rojas-López, J. Nieto-Navarro, E. Rosendo, H. Navarro-Contreras, and M. A. Vidal, *Thin Solid Films* **379**, 1 (2000).
- ¹⁹C. Vigreux, L. Binet, and D. Gourier, *J. Solid State Chem.* **157**, 94 (2001).
- ²⁰V. Yu. Davydov, V. V. Emstev, I. N. Goncharuk, A. N. Smirnov, V. D. Petrikov, V. V. Mamutin, V. A. Vekshin, S. V. Ivanov, M. B. Smirnov, and T. Inushima, *Appl. Phys. Lett.* **75**, 3297 (1999).
- ²¹T. S. Moss, *Proc. Phys. Soc. London, Sect. B* **67**, 775 (1954); E. Burstein, *Phys. Rev.* **93**, 632 (1954).
- ²²I. Hamberg and C. G. Granqvist, *J. Appl. Phys.* **60**, R123 (1986).
- ²³J. S. Thakur, G. W. Auner, D. B. Haddad, R. Naik, and V. M. Naik, *J. Appl. Phys.* **95**, 4795 (2004).
- ²⁴D. Pines and P. Nozieres, *The Theory of Quantum Liquids* (Benjamin, New York, 1966), Vol. I.
- ²⁵E. O. Kane, *J. Phys. Chem. Solids* **1**, 249 (1957).
- ²⁶J. Wu, W. Walukiewicz, W. Shan, K. M. Yu, J. W. Ager III, E. E. Haller, H. Lu, and W. J. Schaff, *Phys. Rev. B* **66**, 201403 (2002).
- ²⁷D. L. Chubb, *Fundamentals of Thermophotovoltaic Energy Conversion* (Elsevier, Amsterdam, Boston, 2007).
- ²⁸P. C. Gibbons, *Phys. Rev. B* **23**, 2536 (1981).